

Chapter 35

Adiabatic Analysis of Spherical and Cylindrical Textured Hydrodynamic Journal Bearing



Mohammad Arif, Saurabh Kango, Dinesh Kumar Shukla, and Nitin Sharma

Abstract The present article highlights on the dual role of viscous heating and surface texturing on the performance of hydrodynamically lubricated finite journal bearing. The Reynolds and energy equations are coupled together, and the solution of these governing equations has been accomplished using finite difference technique. To find more realistic results, JFO boundary conditions are used to solve the Reynolds equation. Based on the investigations reported herein, it is observed that out of two surface textures, the cylindrical texture is the best for improving the load and friction coefficient at high speeds as compared to spherical texture, whereas the improvement in average temperature is highest at low speeds.

Keywords Thermal analysis · JFO boundary condition · Spherical and cylindrical dimpling · Average temperature · Coefficient of friction

List of Symbols

c_r	Radial clearance (μm)
$\bar{F}_{\text{Smooth/Texture}}$	Dimensionless friction force
$f_{\text{Smooth/Texture}}$	Coefficient of friction
g	Switch function
i	Number of nodes in X -direction
j	Number of nodes in Y -direction
k	Number of nodes in Z -direction
I	Number of iterations
N	Shaft speed (rpm)
N_θ	Number of nodes in circumferential direction
N_Z	Number of nodes in axial direction

M. Arif (✉) · S. Kango · D. K. Shukla · N. Sharma
Department of Mechanical Engineering, Dr. B R Ambedkar National Institute of Technology,
Jalandhar 144011, India
e-mail: mohammada.me.18@nitj.ac.in

$N_{I\theta}$	Number of textures in circumferential direction
N_{IZ}	Number of textures in axial direction
p	Bearing pressure (Pa)
P	Dimensionless pressure: $P = \frac{pc_c^2}{\eta RU}$
p_c	Cavitation pressure
R	Shaft radius (m)
r_y	Dimple depth (μm)
r	Dimple radius (m)
T_0	Inlet temperature ($^{\circ}\text{C}$)
T	Lubricant temperature ($^{\circ}\text{C}$)
\bar{T}	Dimensionless temperature: $\bar{T} = \gamma(T - T_0)$
U	Shaft speed (m/s)
u	Lubricant velocity in X -direction (m/s)
w	Lubricant velocity in Z -direction (m/s)
$\bar{W}_{\text{Smooth/Texture}}$	Dimensionless load for smooth and texture bearing = $(W * c_r^2)/(\eta * U * L * R^2)$
θ	Circumferential angle (degree)
γ	Viscosity-temperature index
ϕ	Film content of the lubricant
β	Bulk modulus of the lubricant
ε	Eccentricity ratio
τ	Shear stress (Pa)
ρ	Lubricant density (Kg/m^3)
α	Dissipation number = $\frac{R\gamma\eta_0 U}{\rho c_r^2}$

35.1 Introduction

It is being widely reported in the literature that micro-texturing/dimpling on the surfaces of the tribological elements is proving to be beneficial in terms of reduction in friction and wear at the lubricated interface [1]. Dimples at the mating interface of tribo-elements act as micro-hydrodynamic bearings, which generate the pressure in the lubricating film for supporting the external load efficiently. Moreover, the micro-dimples of texture pattern fabricated on the surfaces of tribo-elements serve as innumerable micro-fluid film bearings. However, these shallow micro-dimples work as lubricant reservoirs, which provide lubricant to spread at the interface of tribo-elements in case of mixed/boundary lubrications. Moreover, these dimples also may act as wear debris/foreign particles [2]. Research on the influences of surface roughness, corrugations, and textures on the bearing performance has been attempted in different forms in the past. Huynh [3–5] carried out numerical analysis for slider bearing with sinusoidal corrugations and concluded that the location of sinusoidal roughness affects the performance of slider bearing strongly. The influence of surface

roughness on journal bearing was studied by Maharshi et al. [6], where authors concluded that the roughness has pronounced influence on the performance of bearing. The effect of positive micro-grooving at different locations on the journal bearing surface has been investigated by Kango and Sharma [7], wherein the authors concluded that the load-carrying capacity is very high in the minimum film thickness region for optimum eccentricity ratio. The authors also performed a comparative study of sinusoidal, full- and half-wave positive micro-grooving and observed that longitudinal sinusoidal roughness is best suited for decreasing the friction force. Kango et al. [8] reported that the half-wave negative roughness texture enhances the bearing performance more in comparison with full-wave texture on the journal bearing surface. In other works, Sharma et al. [9] studied the combined effect for a finite journal bearing with JFO boundary conditions of spherical textures with couple stress fluids and reported that load-carrying capacity gets increased with couple stresses at different eccentricity ratios. However, with textures, the increase in load-carrying capacity was noted significant only at low eccentricity ratios. Yamada et al. [10, 11] studied the effect of square dimples on static and dynamic characteristics of journal bearing and concluded that static and dynamic characteristics of journal bearing get improved by square dimples. Wang et al. [12] carried out thermo-hydrodynamic analysis of journal bearing with surface texturing and concluded that the textured bearing gave a higher load-carrying capacity, a lower maximum oil pressure, and a lower oil temperature rise than the un-textured bearing based on an optimal design of texture. Tala-Ighil et al. [13, 14], Cupillard et al. [15], Brizmer and Kligerman [16] have studied the roles of different surface dimpling (spherical and cylindrical) in their respective studies under certain assumptions and considerations for hydrodynamic journal bearings. The authors concluded that the partial surface texturing has a great influence on the performance characteristics of the journal bearings. However, these researchers have presented their respective investigations for isothermal operating conditions. Moreover, the authors of the present paper could not notice any research paper dealing with the analysis of surface dimpled/textured journal bearings using the JFO boundary condition by incorporating viscous heat dissipation in the lubricating film. Thus, the objective of this paper is to present a numerical model for the thermal analysis of hydrodynamically lubricated journal bearing having spherical and cylindrical surface dimpling on the bearing surface by incorporating realistic JFO boundary condition in order to satisfy the mass conservation in cavitation zone.

35.2 Theoretical Analysis

35.2.1 *Mathematical Model*

Schematic diagram of journal bearing adopted in the present investigation with coordinate system is shown in Fig. 35.1. The circumferential length in the X -direction, length in Z -direction, and film thickness in Y -direction are represented by $R\theta$, L , and

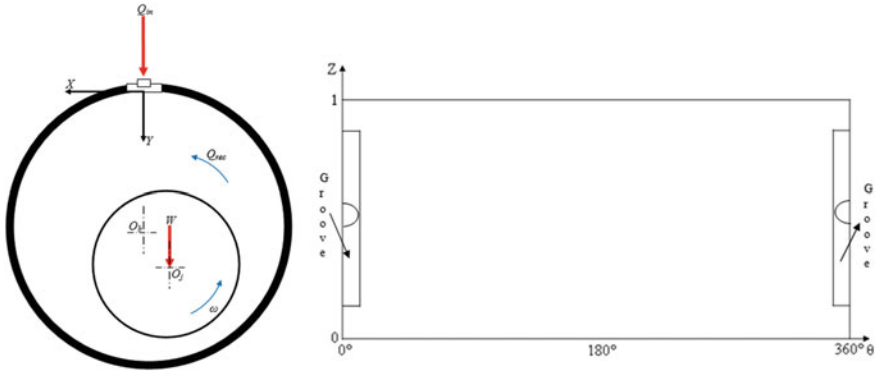


Fig. 35.1 Schematic diagram of journal bearing

H , respectively. It is essential to mention here that the proposed investigation has been carried out for incompressible and steady-state laminar flow of lubricating oil. Moreover, body and inertia forces have been ignored. The expression for lubricating film thickness is defined as follows:

$$H = (1 + \varepsilon \cos \theta) + \Delta h(\theta, Z) \tag{35.1}$$

where $\Delta h(\theta, Z)$, the dimensionless film thickness component due to different surface dimples, has been adopted from Tala-Ighil et al. [13, 14] and is computed as follows:

$$\begin{aligned} \Delta h(\theta, Z)_{\text{cylindrical}} &= r_y \\ \Delta h(\theta, Z)_{\text{spherical}} &= \frac{r_y}{r} \sqrt{r^2 - (R\theta - x_c)^2 - (z - z_c)^2} \end{aligned}$$

where ‘ ε ’ is the eccentricity ratio.

Reynolds equation suggested by Elrod [17] for incorporating the cavitation/mass conservation feature is used in computation as follows:

$$\frac{\partial}{\partial \theta} \left(\frac{H^3 g}{\bar{\eta}} \frac{\partial \phi}{\partial \theta} \right) + \left(\frac{R}{L} \right)^2 \frac{\partial}{\partial Z} \left(\frac{H^3 g}{\bar{\eta}} \frac{\partial \phi}{\partial Z} \right) = \frac{6}{\bar{\beta}} \frac{\partial(\phi H)}{\partial \theta} \tag{35.2}$$

The switch function (g) is taken from the works of Elrod [17] as follows:

$$g = 0 \quad \phi < 1 \quad \text{and} \quad g = 1 \quad \phi < 1 \tag{35.3}$$

The pressure in the full film region is determined from the following relation:

$$p = p_c + \beta(\phi - 1) \tag{35.4}$$

For accounting the temperature rise in the lubricating film due to viscous heat dissipation, the following energy equation is used [18]:

$$\bar{u} \frac{\partial \bar{T}}{\partial \theta} + \bar{w} \frac{\partial \bar{T}}{\partial Z} \left(\frac{R}{L} \right) = \frac{\alpha \bar{\eta}}{H^2} \left[\left(\frac{\partial \bar{u}}{\partial Y} \right)^2 + \left(\frac{\partial \bar{w}}{\partial Y} \right)^2 \right] \tag{35.5}$$

In this investigation, it is assumed that the heat generated within the lubricating film is completely carried away by the lubricant through convection mode of heat removal. Moreover, herein, temperature variation across the lubricating film has been neglected.

Lubricating oil viscosity variation with temperature is taken by the following expression:

$$\bar{\eta} = \exp(-\bar{T}) \tag{35.6}$$

Load-carrying capacity (\bar{W}), friction force (\bar{F}), and coefficient of friction (f) are computed using the following relations:

$$\bar{W}_{\text{texture}} = \int_0^1 \int_0^{2\pi} P d\theta dZ \tag{35.7}$$

$$\bar{F}_{\text{texture}} = \int_0^1 \int_0^{2\pi} \bar{\tau} d\theta dZ \tag{35.8}$$

$$f_{\text{texture}} = \frac{\bar{F}_{\text{texture}}}{\bar{W}_{\text{texture}}} \tag{35.9}$$

$$\bar{T}_{\text{average}_{\text{texture}}} = \frac{\sum \bar{T}(i, k)}{N_\theta \times N_Z} \tag{35.10}$$

$$\text{Percentage variation in } \bar{W} = \frac{\bar{W}_{\text{texture}} - \bar{W}_{\text{smooth}}}{\bar{W}_{\text{smooth}}} \times 100 \tag{35.11}$$

$$\text{Percentage variation in } f = \frac{f_{\text{texture}} - f_{\text{smooth}}}{f_{\text{smooth}}} \times 100 \tag{35.12}$$

$$\text{Percentage variation in } \bar{T}_{\text{average}} = \frac{\bar{T}_{\text{average}_{\text{texture}}} - \bar{T}_{\text{average}_{\text{smooth}}}}{\bar{T}_{\text{average}_{\text{smooth}}}} \times 100 \tag{35.13}$$

Discretization of Reynolds and energy equations has been done using finite difference method. In the present work, coupled solution of the governing equation is achieved for evaluation of pressure and temperature in the domain. Gauss–Seidel iterative method with modified switch function algorithm purposed by Fesanghary and Khonsari [19] is adopted for speedy convergence. Following convergence criteria

are used in acquiring the numerical results of the domain variables:

$$\sum \sum \left| \frac{(P_{ik})_N - (P_{ik})_{N-1}}{(P_{ik})_N} \right| < 10^{-06} \quad (35.14)$$

$$\sum \sum \left| \frac{(\bar{T}_{i,k})_N - (\bar{T}_{i,k})_{N-1}}{(\bar{T}_{i,k})_N} \right| < 10^{-08} \quad (35.15)$$

where i , k , and N represent the number of nodes in X -direction, Z -direction, and number of iterations, respectively. The numerical results presented in this paper are tested for grid independence and have been generated using the grid size (217, 70). Corresponding to this grid size (217, 70), a dimple has about 100 nodes. Results negligibly varied if nodes were kept more than 100 in a dimple.

35.3 Results and Discussion

35.3.1 Validation of the Smooth Bearing Model

Numerical results have been presented for different input parameters of journal bearing and lubricating oil mentioned in the captions of various figures reported herein. Moreover, the input parameters used in this work are also presented in Table 35.1. Figure 35.2a, b presents comparisons of numerical results for pressure and temperature variations achieved from the proposed mathematical model with the works of Elrod [17] and Jang and Chang [18], respectively. Good correlations between both the results can be seen in these figures. This develops a fairly reasonable confidence in the proposed numerical model.

35.3.2 Influence of Number of Dimples in Circumferential Direction

Brizmer and Kligerman [16] have investigated the influence of spherical texture on the performance of short and infinite bearing at low and high eccentricity ratios. The authors concluded that the more improvement in load-carrying capacity is achieved only at a low eccentricity ratio with partial surface texturing. Therefore, the present work is based on low eccentricity ratio ($\varepsilon = 0.3$).

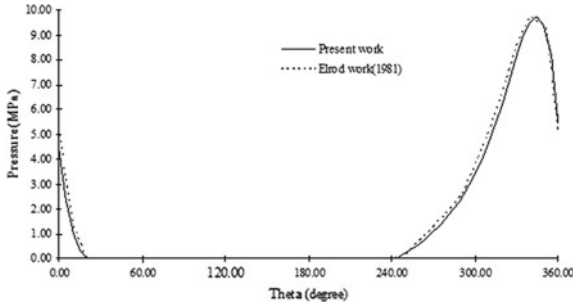
The schematic representation for textures is shown in Fig. 35.3 for one and ten number of dimples in circumferential direction. It is essential to mention here that in the surface texturing, 3D shape of the micro-dimple is spherical and cylindrical as shown in Fig. 35.4a–e. Figures 35.5a–e and 35.6a–e depict the 3D representation of the dimensionless thermal pressure and temperature for both the cases (smooth

Table 35.1 Input parameters for the present work

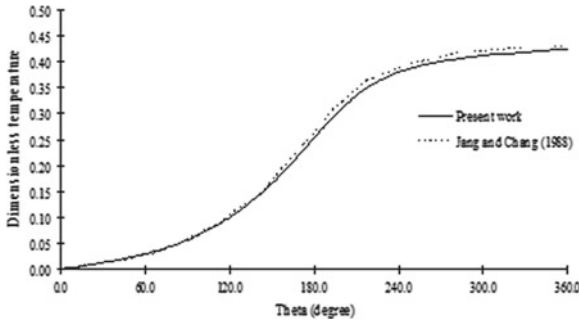
Sr. No.	Initial parameters	Values	Unit
1	Eccentricity ratio (ϵ)	0.3	
2	Dynamic viscosity (η)	0.08	(Pa.s)
3	Shaft speed (N)	1000, 3000, 5000	(rpm)
4	Radial clearance (Cr)	50	(μm)
5	Shaft radius (R)	0.02	(m)
6	Bearing length (L)	0.04	(m)
7	Specific heat (cp)	1840	(J/kg °C)
8	Lubricant density (ρ)	881.6	(Kg/m ³)
9	Nodes (N_θ and N_z)	217 and 70	—
10	$d\theta$ and dz	0.00058 and 0.00058	(m)
11	Dimple radius (r)	0.0028	(m)
12	Area density of dimple (S_p)	0.68	
13	a	0.00058	(m)
14	b	0.00058	(m)
15	L_x	0.006	(m)
16	L_z	0.006	(m)
17	Inlet temperature	40	(°C)
18	Viscosity-temperature index	0.0315	(°C ⁻¹)

and dimpled). In the present study, the influence of location of surface texture in the circumferential direction, and dimple depth on performance parameters of journal bearing (load, friction coefficient, and average temperature) is investigated. In this study, the number of dimples in axial direction has been kept constant ($N_{tZ} = 6.0$) throughout, whereas, the numbers of dimples in the circumferential direction vary from 1 to 10 as shown in Fig. 35.3b–e, and this has been considered in the convergent zone from 0 to 210 degrees. Moreover, in this investigation, the textured surface area fraction is 0.68.

Figures 35.7, 35.8 and 35.9 show the influence of number of dimples ($N_{t\theta}$) for both textured bearings (spherical and cylindrical) with and without constant viscosity (isothermal and thermal). It has been observed that the percentage load increases up to 4.0, and after this value, it starts to decrease as shown in Fig. 35.7 for both the cases. More reduction in % load is achieved for cylindrical texture at higher number of dimples. The improvement in % load for spherical and cylindrical textures is 3.901% and 3.828%, respectively, at $N_{t\theta} = 4.0$. Figure 35.8 elucidates similar behaviour in terms of improvement in friction coefficient for both the cases. This may be due to the fact that friction coefficient is the ratio of load and friction force, as and when the load increases, the friction force gets increased. Therefore, the friction coefficient shows more reduction at $N_{t\theta} = 4.0$, i.e. up to 4.809 and 5.075% for



(a) Comparison of pressure results for smooth journal bearing [D=62.8mm, $h_0=55\mu\text{m}$, L/D=10, Location of grooves= 60° and 240°, Number of grooves=2, U=19.7m/s, $\epsilon=0.8$, $\eta=0.0035$ Pa.



(b) Comparison of the dimensionless temperature for smooth bearing [$C_p=1840$ J/Kg/°C, $cr=100\mu\text{m}$, D=100 mm, L/D=1.0, N=1000 rpm, $\epsilon=0.6$, $\eta=0.0416$ Pa.s, $\gamma=0.0315/^\circ\text{C}$]

Fig. 35.2 Validation of the proposed model with the published results of researchers

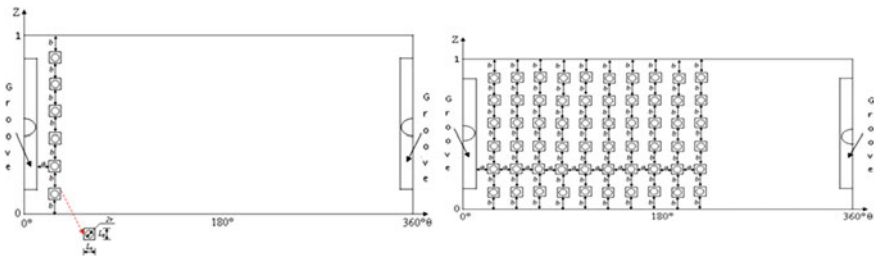


Fig. 35.3 Schematic diagram for textured hydrodynamic journal bearing

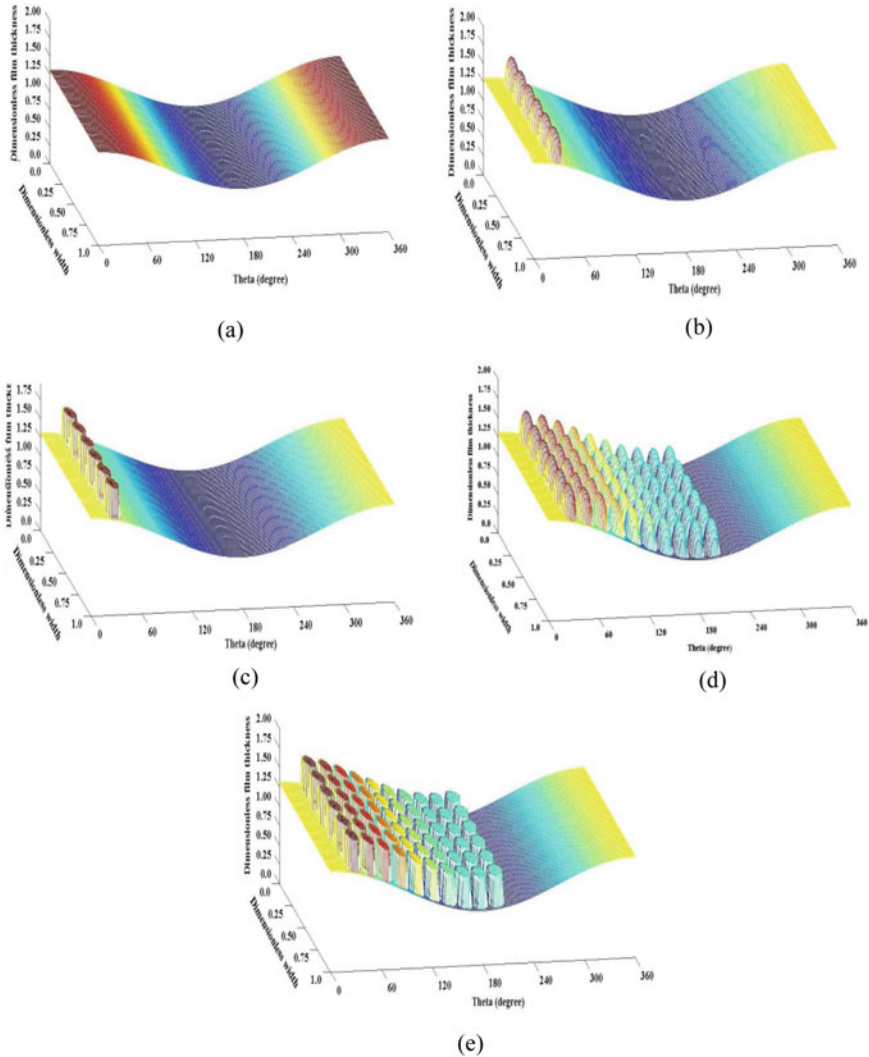


Fig. 35.4 Lubricant film thickness for configurations of smooth, spherical, and cylindrical textured bearing surface [$N = 1000$ rpm, $r_y = 20 \mu\text{m}$, $N_{t\theta} = 1.0$ to 10.0 , $N_{tZ} = 6.0$]

spherical and cylindrical textures, respectively. Considerably higher reduction in average temperature is achieved for cylindrical texture (4.218%) as compared to spherical texture (3.258%). Thus, it is observed that the cylindrical texture improves the bearing performance more in terms of friction, and average temperature reduction as compared to spherical texture for constant geometry and similar input parameters.

There is less variation in values of load and friction coefficient for isothermal and thermal cases as shown in Figs. 35.7a, b, and 35.8a, b. The main reason behind this

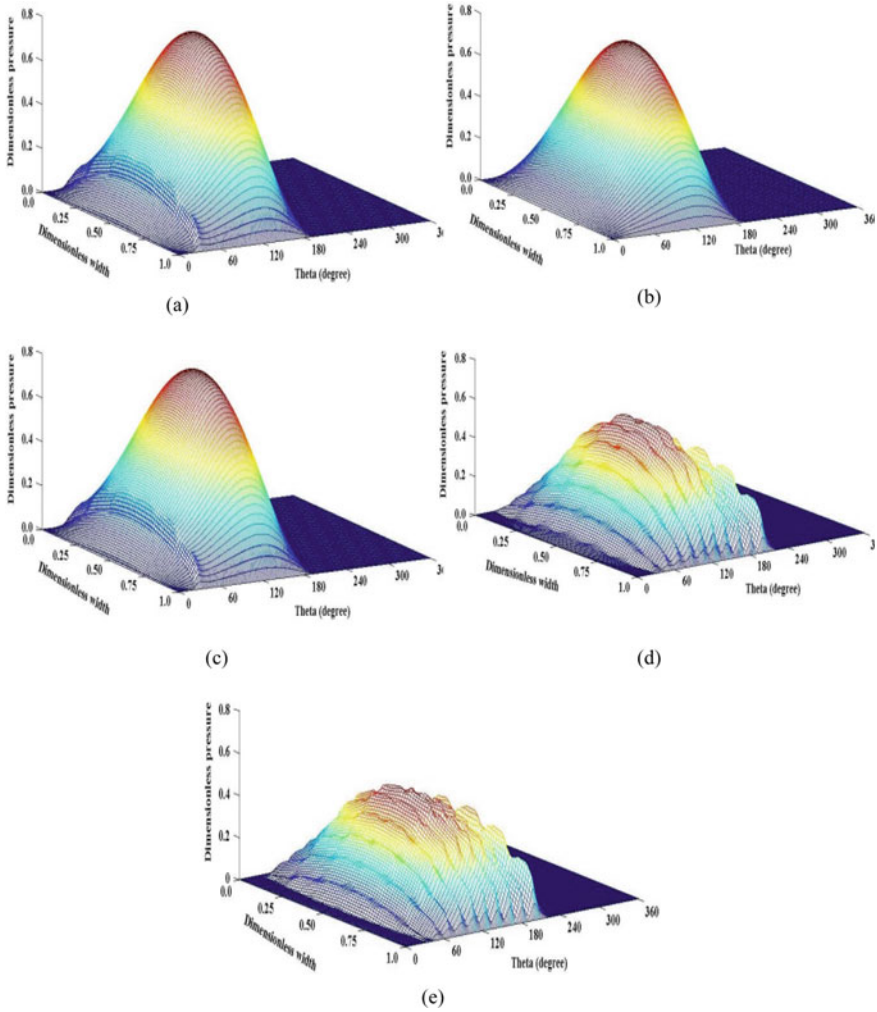


Fig. 35.5 Lubricant pressure (with thermal effect) for configurations of smooth, spherical, and cylindrical textured bearing surface [$N = 1000$ rpm, $r_y = 20 \mu\text{m}$, $N_{t\theta} = 1.0$ to 10.0 , $N_{tZ} = 6.0$]

is lower journal speed (1000 rpm) as at low speeds, the heating effect due to sliding of intermediate lubricant layers on viscosity is less and leads to less degradation of the lubricant. Therefore, the percentage variation in performance parameters of the bearing is almost the same for isothermal and thermal cases (3.828 and 3.351% reduction in friction coefficient for isothermal and thermal cases, respectively). As the best performance has been observed to be corresponding to four numbers of dimples in circumferential direction, i.e. $N_{t\theta}$ value, hence, for further analysis, four numbers of dimples in the circumferential direction have been taken.

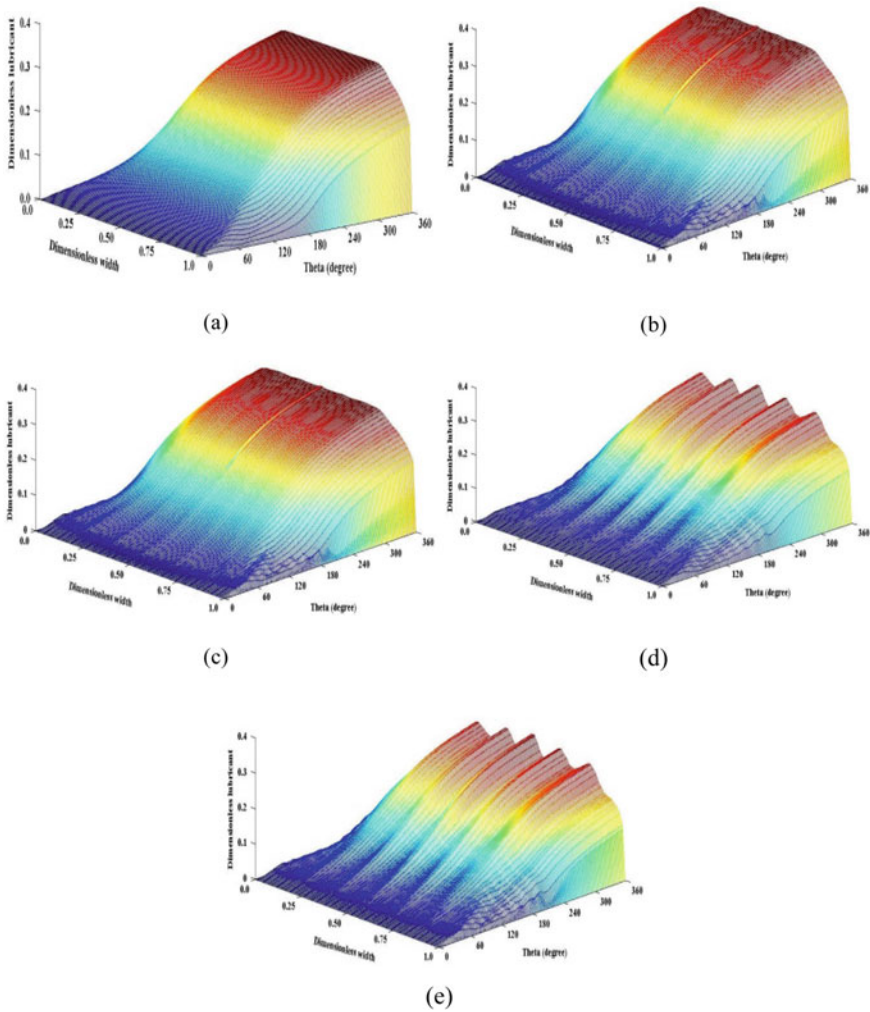


Fig. 35.6 Lubricant temperature for configurations of smooth, spherical, and cylindrical textured bearing surface [$N = 1000$ rpm, $r_y = 20 \mu\text{m}$, $N_{I\theta} = 1.0$ to 10.0 , $N_{Iz} = 6.0$]

35.3.3 Influence of Journal Speed

The values in terms of percentage variation for thermal case at low speeds are almost the same due to less heat dissipation and corresponding lower temperature generation as discussed earlier. However, at higher speeds, the influence of journal speed with both textured bearings is visible as presented in Table 35.2. The percentage improvement in performance parameters is approximately same for all journal speeds in isothermal case. This is happening due to constant lubricant viscosity in this case.

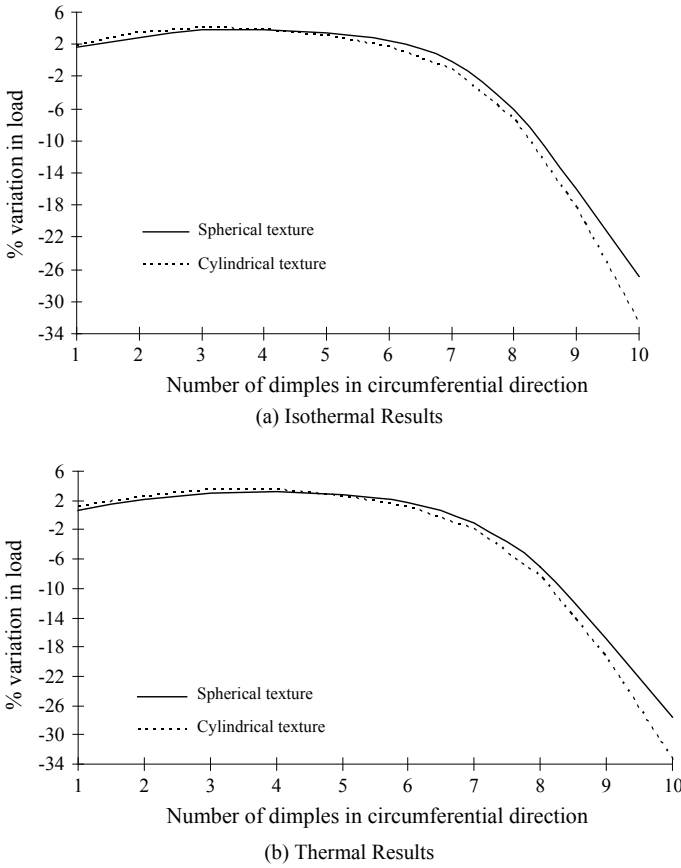
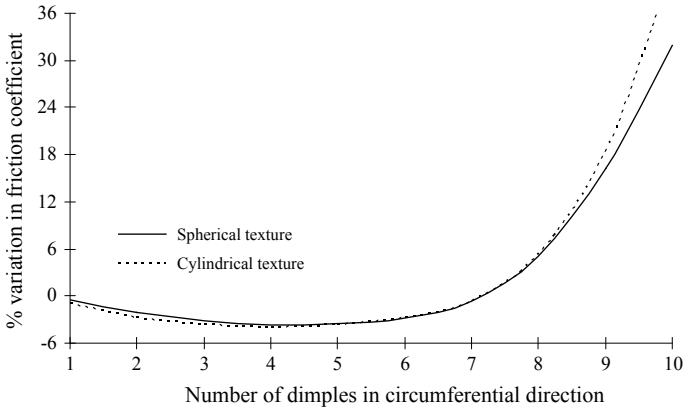


Fig. 35.7 Comparison of different textures on the basis of % variation in load with change in $N_{t\theta}$ [$N = 1000$ rpm, $r_y = 20 \mu\text{m}$, $N_{t\theta} = 1.0$ to 10.0 , $N_{tZ} = 6.0$]

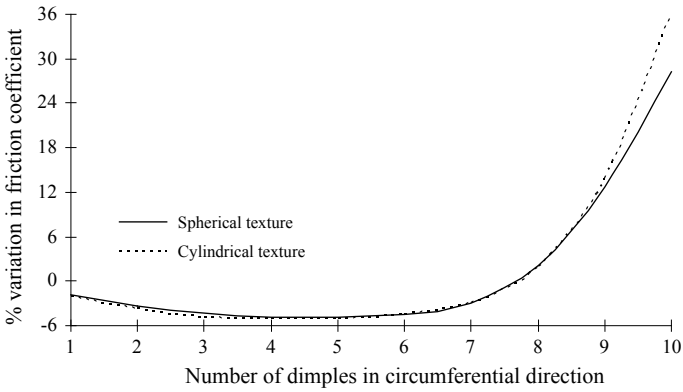
However, there more difference is achieved in terms of percentage improvement with change of journal speed for thermal case. Two main observations from Table 35.2 are given below:

1. Higher percentage reduction up to 5.73% in friction coefficient is seen for cylindrical texture at high speed (5000 rpm).
2. Higher percentage reduction up to 4.22% in average temperature has been observed for cylindrical texture at low speed (1000 rpm).

It is therefore indicative that the journal speed influences the performance of textured bearings.



(a) Isothermal Results



(b) Thermal results

Fig. 35.8 Comparison of different textures on the basis of % variation in friction coefficient with change in $N_{t\theta}$ [$N = 1000$ rpm, $r_y = 20 \mu\text{m}$, $N_{t\theta} = 1.0$ to 10.0 , $N_{tZ} = 6.0$]

35.3.4 Influence of Dimple Depth

The percentage variation due to thermal conditions in load, friction coefficient, and average temperature with different dimple depths for textured bearings is shown in Figs. 35.10, 35.11, and 35.12, respectively. The load-carrying capacity increases with increasing the dimple depth up to $15 \mu\text{m}$ for cylindrical texture (3.794%, 5.879%, and 6.537% at 1000, 3000, and 5000 rpm, respectively, at $15 \mu\text{m}$) and up to $20 \mu\text{m}$ for spherical texture (3.211%, 5.229%, and 5.807% at 1000, 3000, and 5000 rpm, respectively, at $20 \mu\text{m}$) as depicted in Fig. 35.10. The corresponding reduction in friction coefficient is 4.265, 5.764, and 6.008% for cylindrical texture at $15 \mu\text{m}$ and 3.620, 5.128, and 5.342% for spherical texture at $20 \mu\text{m}$ with three different speeds,

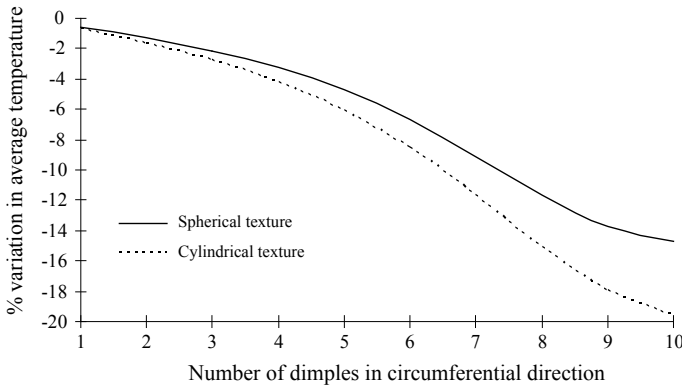


Fig. 35.9 Comparison of different textures on the basis of % variation in average temperature with change in $N_{t\theta}$ [$N = 1000$ rpm, $r_y = 20 \mu\text{m}$, $N_{t\theta} = 1.0$ to 10 , $N_{tZ} = 6.0$]

Table 35.2 Comparison of % variation in load, friction coefficient, and average temperature for spherical and cylindrical textures with change in journal speed [$r_y = 20 \mu\text{m}$, $N_{t\theta} = 4.0$, $N_{tZ} = 6.0$]

Journal speed (rpm)	Texture	% variation in load	% variation in friction coefficient	% variation in average temperature
<i>Isothermal results</i>				
1000	Spherical	+3.901	-4.809	—
	Cylindrical	+3.828	-5.075	—
3000	Spherical	+3.895	-4.734	—
	Cylindrical	+3.821	-4.998	—
5000	Spherical	+3.895	-4.729	—
	Cylindrical	+3.821	-4.991	—
<i>Thermal results</i>				
1000	Spherical	+3.211	-3.620	-3.258
	Cylindrical	+3.351	-3.985	-4.218
3000	Spherical	+5.229	-5.128	-3.068
	Cylindrical	+5.460	-5.447	-3.954
5000	Spherical	+5.807	-5.342	-2.913
	Cylindrical	+6.218	-5.733	-3.762

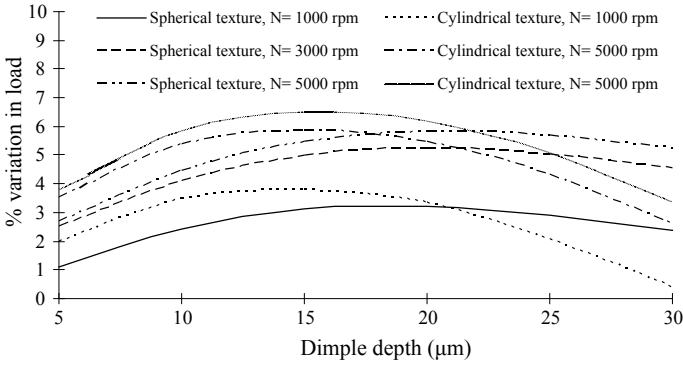


Fig. 35.10 Comparison of different textures on the basis of % variation in load with change in dimple depth [$N = 1000$ rpm, $r_y = 20 \mu\text{m}$, $N_{t\theta} = 4.0$, $N_{tZ} = 6.0$]

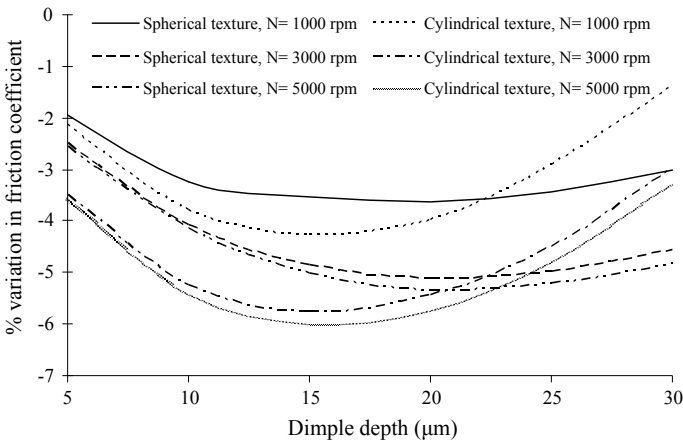


Fig. 35.11 Comparison of different textures on the basis of % variation in friction coefficient with change in dimple depth [$N = 1000$ rpm, $r_y = 20 \mu\text{m}$, $N_{t\theta} = 4.0$, $N_{tZ} = 6.0$]

respectively, as observed from Fig. 35.11. The percentage reduction in average temperature is 3.658, 3.438, and 3.268% for cylindrical texture and 3.258, 3.068, and 2.913% for spherical textures for different speeds as shown in Fig. 35.12.

It can therefore be concluded from above discussion that the optimal value of dimple depth for cylindrical and spherical textures is 15 and 20 micrometers, respectively, at all three journal speeds. It is also observed that the percentage improvement is less for cylindrical texture when compared with spherical texture at high dimple depths.

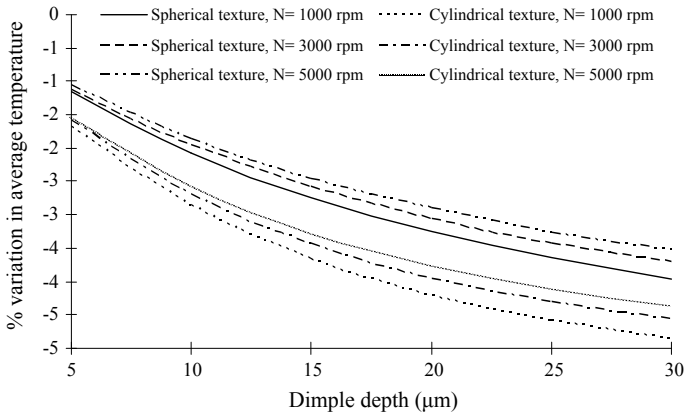


Fig. 35.12 Comparison of different textures on the basis of % variation in average temperature with change in dimple depth [$N = 1000$ rpm, $r_y = 20$ μm, $N_{t\theta} = 4.0$, $N_{tZ} = 6.0$]

35.4 Conclusions

In the present work, a comparative study has been reported between two different surface textures (spherical and cylindrical) for isothermal and thermal cases with different journal speeds and dimple depths.

Following are the broad outcomes of this study:

1. The number of dimples in circumferential direction has a great influence on the bearing performance characteristics. From the present study, four numbers of dimples in circumferential direction at inlet zone have been found to be best for improving the load, friction coefficient, and average temperature.
2. The percentage variation of thermal results is more at higher speeds as compared to isothermal results.
3. Higher reduction in friction coefficient is achieved at high speeds. However, the reduction in average temperature is high at low speed.
4. The optimum value of dimple depth is different for both the textured bearings.

It has been observed that out of two surface textures, the cylindrical texture is the best for improving the load and friction coefficient at high speeds as compared to spherical texture, whereas the improvement in average temperature is highest at low speeds.

References

1. Etsion, I.: Laser surface texturing and applications In: Nikas, G.K. (ed) Recent developments in wear prevention, friction and lubrication. 137–157 (2010)
2. Etsion, I.: State of the art in laser surface texturing. ASME J. Tribol. **127**, 248–253 (2005)

3. Huynh, B.P.: Numerical study of slider bearings with limited corrugation. *ASME J. Tribol.* **127**, 582–595 (2005)
4. Huynh, B.P.: Numerical investigation of slider bearings with limited corrugation and power-law Lubricant. In: Proceedings of the ASME 2011 International Mechanical Engineering Congress & Exposition IMECE2011, Denver, Colorado, USA
5. Huynh, B.P.: Thermal effects in slider bearings with limited corrugation and power-law lubricant. In: Proceedings of the ASME 2012 International Mechanical Engineering Congress & Exposition IMECE2012, Houston, Texas, USA
6. Maharshi, K., Mukhopadhyay, T., Roy, B., Roy, L., Dey, S.: Stochastic dynamic behaviour of hydrodynamic journal bearings including the effect of surface roughness. *Int. J. Mech. Sci.* **142**, 370–383 (2018)
7. Kango, S., Sharma, R.K.: Studies on the influence of surface texture on the performance of hydrodynamic journal bearing using power law model. *Int. J. Surf. Sci. Eng.* **4**(4/5/6): 505–524 (2010)
8. Kango, S., Singh, D., Sharma, R.K.: Numerical investigation on the influence of surface texture on the performance of hydrodynamic journal bearing. *Meccanica* **47**, 469–482 (2012)
9. Sharma, N., Kango, S., Tayal, A., Sharma, R.K., Sunil: Investigation on the influence of surface texturing on a couple stress fluid based journal bearing by using JFO boundary conditions. *Tribol. Trans.* **59**, 579–584 (2016)
10. Yamada, H., Taura, H., Kaneko, S.: Numerical and experimental analyses of the dynamic characteristics of journal bearings with square dimples. *J. Tribol.* **140**(1), 011703 (2018)
11. Yamada, H., Taura, H., Kaneko, S.: Static characteristics of journal bearings with square dimples. *J. Tribol.* **139**(5), 051703 (2017)
12. Wang, L., Han, Z., Chen, G., Su, H.: Thermo-hydrodynamic analysis of large-eccentricity hydrodynamic bearings with texture on journal surface. *Proc. Inst. Mech. Eng. Part C: J. Mech. Eng. Sci.* **232**(19), 3564–3569 (2018)
13. Tala-Ighil, N., Maspeyrot, P., Fillon, M., Bounif, A.: Effects of surface texture on journal bearing characteristics under steady state operating conditions. *Proc. Inst. Mech. Eng. Part C: J. Eng. Tribol.* **221**, 623–633 (2007)
14. Tala-Ighil, N., Fillon, M., Maspeyrot, P.: Effect of textured area on the performances of a hydrodynamic journal bearing. *Tribol. Int.* **44**, 211–219 (2011)
15. Cupillard, S., Glavatskih, S., Cervantes, M.J.: CFD analysis of journal bearing with surface texturing. *Proc. Inst. Mech. Eng. Part J: J. Eng. Tribol.* **222**, 97–107 (2008)
16. Brizmer, V., Kligerman, Y.: A laser surface textured journal bearing. *ASME J. Tribol.* **134**, 031702-1-9 (2012)
17. Elrod, H.G.: A cavitation algorithm. *ASME J. Tribol.* **103**, 350–354 (1981)
18. Jang, J.Y., Chang, C.C.: Adiabatic analysis of finite width journal bearings with non-newtonian lubricants. *Wear* **122**, 63–75 (1988)
19. Fesanghary, M., Khonsari, M.M.: A modification of the switch function in the elrod cavitation algorithm. *ASME J. Tribol.* **133**, 024501-1-024501-4 (2011)